**Journal of Hard Tissue Biology 30[2] (2021) 165-174**

CODEN-JHTBFF, ISSN 1341-7649

## Original

# A Study of Bone Formation around Titanium Implants Using Frozen Sections

**Komei Kawamoto[1)], Takuma Suzuki[1)], Takatoshi Nagano[1)], Tadafumi Kawamoto[2)] and Kazuhiro Gomi[1)]**

*[1)] Department of Periodontology, School of Dental Medicine, Tsurumi University, Yokohama, Japan*
*[2)] Radioisotope Research Institute, Tsurumi University, Yokohama, Japan*
(Accepted for publication, March 1, 2021)

Abstract: Titanium is most widely used for implants. Almost all the histological studies of the implants have been carried out with polished specimens and the use of frozen sections are challenging. This study focused to define the formation process of bone around titanium with frozen sections made from tissue implanted with a commercially pure titanium foil (Ti-foil). We inserted the Ti-foil with a 30-μm thickness into rat femurs and extracted it after 1, 3, 5, 7, 10, 15, and 30 days. After freezing, they were sliced into 3-μm thick serial frozen sections and the sections were used for hematoxylin and eosin (H&E) staining, Masson trichrome staining, Alizarin Red S staining, enzymatic staining (ALPase and TRAPase), immunostaining (osteopontin, osteocalcin, and collagen type I), and elemental analysis. At 1 day after the implantation, the area around the Ti-foil was filled with blood and there are no collagen fibers and no proliferated cells in the area. At 3 days, the new collagen fibers were observed on the marrow side of the blood clot. The proliferated cells were observed around the fibers and they were positive for immunostaining to osteopontin, osteocalcin, and collagen type I. After 5 days, calcium precipitation was observed on the newly formed collagen fibers. After 7 days, the calcification progressed and started to reach the Ti-foil surface. After 10 days, calcification progressed to the area around the Ti-foil. At 15 days, a remarkable bone resorption appears on the marrow side. At 30 days, further resorption was observed and bony tissue was seen on the Ti-foil surface only. These results clearly showed that the bone around the Ti-foil is formed after undergoing the blood clotting process around the Ti-foil, osteoblast and fibroblast proliferation, calcium precipitation on the collagen fibers, bone formation around the Ti-foil, and bone resorption by osteoclasts.

Key words: Frozen section, Titanium, Wound healing, Bone, Implant

## Introduction

Previously, metallic materials such as titanium, stainless steel, and cobalt-chrome alloy have been used in implants[1-5)]. Ceramic materials such as carbon, alumina, and calcium phosphate have also been used[6-9)]. Of these materials, titanium offers superior mechanical strength and corrosion resistance as well as superior affinity with bone. Consequently, it is the most widely used implant material.

Studies investigating the efficacy of titanium as an implant material have comprised *in vitro* experiments examining protein adsorption ability, cell induction ability, cell adhesion ability, cell proliferative ability, and calcification ability etc. on titanium[10-16)]. Meanwhile, *in vivo* experiments have involved studies of bone tissue formation around the titanium after the implantation of titanium in experiments using animals, such as rats or rabbits[17-21)]. Bone formation can be observed three-dimensionally by directly viewing the titanium implant materials using micro computed tomography (micro-CT) or by observing sections prepared from the resin-embedded sections[22-25)]. While micro-CT has the advantage of offering simple, three-dimensional observation of bone formation around the titanium, it does not offer sufficient resolution for observing initial tissue changes after titanium implantation, initial calcification, and the bone tissue formation process near the titanium. Furthermore, it cannot reveal soft tissue changes that occur after titanium implantation or gene expression changes associated with tissue changes. While observing the resin-embedded section surfaces makes it possible to observe the bone tissue formation state around the titanium, it is challenging to determine the histological changes after titanium implantation due to limitations on histological staining, histochemical staining, and enzyme histochemical staining as well as resolution issues. There is also the issue of the inability to perform immunohistochemical staining or gene expression analysis[26)]. Therefore, the histological and biochemical changes that occur directly after titanium implantation have not been sufficiently revealed.

We believe that these issues could be resolved by using frozen sections of titanium-implanted tissues. Although it was impossible to use conventional methods to prepare frozen sections from hard tissue, Kawamoto reported a method for preparing frozen sections of hard tissues by using a strong adhesive tape and disposable tungsten carbide blade[27, 28)]. The sections prepared by the method can be used in various types of research, such as histological studies, histochemical studies, enzyme histochemical studies, immunohistochemical studies, genetic histochemical studies, gene expression analysis, matrix-assisted laser desorption ionization mass spectrometry imaging (MALDI-MSI), and elemental analysis. Furthermore, it has been reported that they can be used in studies from a macro to micro level[29-32)].

In this study, we tried to make frozen sections from titanium implant tissue and then examined the bone formation process around the titani-

Correspondence to: Dr. Kazuhiro Gomi, Tsurumi University, School of Dental Medicine, Department of Periodontology, 2-1-3, Tsurumi, Tsurumi-ku, Yokohama 230-8501, Japan; Tel: +81-45-580-8431; Fax: +81-45-580-8431; E-Mail: gomi-k@tsurumi-u.ac.jp

um implant tissue using the frozen sections made by the procedures.

## Materials and Methods

### *Titanium foil selection*

Pieces of pure titanium foil with 10, 20, 30, and 50 μm thicknesses (Japan Industrial Specification H4600. 99.9 mass% Ti, Grade 2, Furuuchi Chemical Corp., Tokyo, Japan) were prepared to select the appropriate titanium foil thickness. Each titanium foil piece was fixed in an embedding medium (SCEM, SECTION-LAB Co. Ltd. Japan) in cooled hexane (−90°C). The frozen specimens were cut with a disposable tungsten carbide blade (SL-T30UF, SECTION-LAB Co. Ltd. Japan) installed in a cryomicrotome (CM3050S, LEICAMICROSYSTEMS GmbH, Germany). Although we were able to cut titanium foil specimens at a thickness of 30 μm or below, we were unable to constantly cut a 50-μm titanium foil piece owing to the damage in the blade. The 30- and 50-μm titanium foils were easy to handle. Based on these results, we used the titanium foil with a 30-μm thickness for our study.

### *Implant surgery*

Animal experiments were approved by the Institutional Animal Care Committee of Tsurumi University School of Dental Medicine (Certificate Number: 24A001). A total of 21 Wistar rats (10-week-old male, weighing 290–310 g) were used. The rat was injected abdominally with pentobarbital sodium (0.1 ml/100 g body weight, Somnopentyl, Kyouritsu Co. Ltd. Japan) as a preparatory anesthesia, and implantation surgery was subsequently performed under general inhalation anesthesia with a 4% isoflurane and oxygen mixture, which was eventually reduced to 2% isoflurane during the surgical manipulation. Local anesthesia was performed by xylocaine injection. Both hind limbs were shaved after sterilization with ethanol. A longitudinal incision was developed on the distal surface of the hind limb to expose the femur. A cortical bone defect (1.0 mm × 9.0 mm) was created through the cortex and medulla. The bone defect was created with a diamond disk (8mm in diameter, HORIKO GmbH, Germany) using a gentle surgical technique and continuous internal cooling using physiological saline solution. Next, a titanium foil of 30-μm thickness was cut into pieces of 6.0 mm × 3.0 mm in size and was inserted into the defect, and the incision site was sutured closed (Fig. 1).

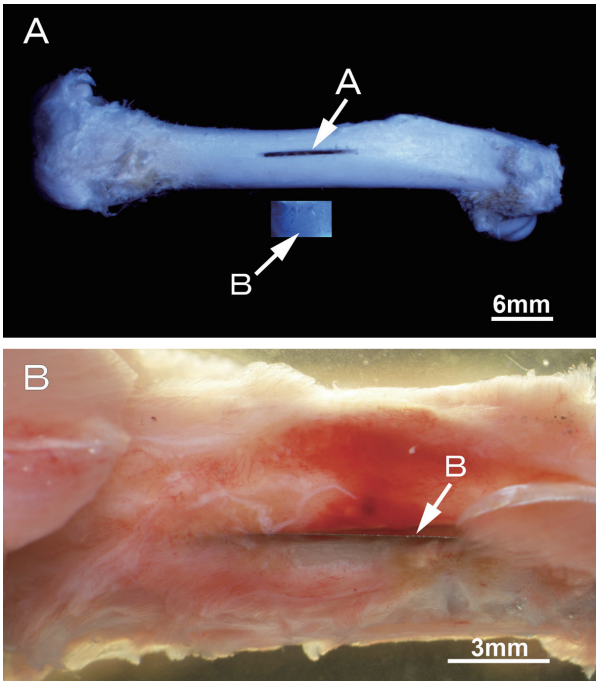


Figure 1. Photograph of the titanium foil implantation. A: Femur opening site (arrow A) and titanium foil (arrow B), B: Rat femur into which the titanium foil is implanted.

### *Frozen section preparation*

The rats implanted with titanium foil were divided into seven groups of three rats each. The rats were euthanized under anesthesia at 1, 3, 5, 7, 10, 15, and 30 days after the titanium foil implantation. After euthanizing, the dissected femurs were fixed with 4% paraformaldehyde [PFA] solution [room temperature] for 24 h. Then, the frozen sections were prepared in accordance with the method described by Kawamoto[28]. The condition for preparing frozen sections was optimized for this purpose. The specimens were completely frozen with cooled hexane (from −46°C to −50°C) to avoid cracks in the sample caused by freezing. Next, the frozen specimens were placed in an embedding medium (SCEM), moved into cooled hexane (−90°C) and completely frozen. The frozen specimens were fixed to a cryomicrotome (CM3050S) kept at −20°C to the cryochamber and −25°C to the sample holder chuck. Then, the specimens were trimmed with a disposable tungsten carbide blade (SL-T30UF). An adhesive film [Cryofilm type 3C (16UF), SECTION-LAB Co. Ltd., Japan] was applied onto the cut surface and then frozen sections of 3–5-μm thickness were made at a slow cutting speed (Fig. 2).

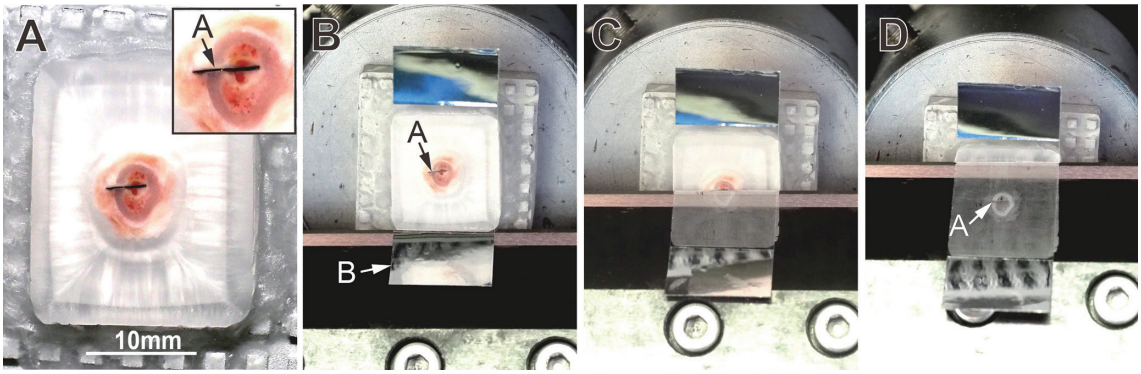


Figure 2. Preparation of 3 μm thick frozen sections from rat femurs implanted with titanium foil. A: Cut surface, B: Cryofilm applied to the cut surface, C: Frozen specimen in cutting, D: Prepared frozen section, arrow A: Titanium foil, arrow B: Cryofilm

***Histological evaluation***

***H&E staining, Masson trichrome staining, and Alizarin Red S staining***

Sections of 3-μm thickness were used for H&E staining, Masson trichrome staining, and Alizarin Red S staining. The frozen sections made with the Cryofilm were taken out of the cryochamber and thawed. After 10 s, they were immersed in 100% ethanol for 10 s. Then, they were placed in 4% PFA for 2 min and rinsed in running water for 4 min.

For the H&E staining, the sections were stained with Carrazzi's Hematoxylin Solution for 90 s and rinsed for 4 min. Next, the sections were stained with 0.2% eosin dissolved in distilled water for 10 s. After staining, the sections were rinsed in 100% ethanol, mounted between the Cryofilm and slide glass with a water-soluble mounting medium (SCMM-R2, SECTION-LAB Co. Ltd. Japan), and then the SCMM-R2 was polymerized using ultraviolet light.

Masson trichrome staining was performed according to the method described by Masson and Martinello et al.[33, 34]. First, the sections that were processed in the same procedure as that described above were stained for 90 s with Carrazzi's Hematoxylin Solution before being rinsed with water. Next, they were rinsed in 1% acetic acid water and stained for 1 min with 0.75% Orange G. Similarly, after rinsing them in 1% acetic acid water, they were stained for 5 min with the Masson's Solution B (Azocarmine G). Subsequently, they were rinsed with 1% acetic acid water, soaked for 15 s in 2.5% phosphotungstic acid hydrate, rinsed in 1% acetic acid water, and stained for 10 s with Aniline blue. After rinsing the stained sections with 100% ethanol, the sections were preserved with SCMM-R2 as shown above.

For Alizarin Red S staining, 0.1% Alizarin Red S solution was dropped on the sections stained for 10 s. Next, after washing with 100% ethanol, the specimens were also preserved by mounting them with SCMM-R2.

***ALPase and TRAPase staining***

ALPase activity was performed according to the method described by Burstone[27, 35]. First, a reaction solution, in which Fast Blue RR Salt (5 mg) and Naphthol AS-MX phosphate (30 mg) were dissolved in a 50-ml of sodium acetate buffer solution (pH 8.31, 0.1 M), was dropped on the 5-μm thick sections and were stained for 5 min. For TRAPase activity, 50 ml of acetate buffer solution (pH 5.2, 0.1 M) added with tartaric acid (2.0 M) was mixed with Fast Red Violet LB Salt (5 mg) and Naphthol AS-MX phosphate (30 mg). This dye solution was dropped on the 5-thick sections and stained for 10 min. The stained sections were mounted with SCMM-R1.

***Immunostaining and DAPI (4', 6-Diamidino-2-phenylindole) staining***

First, Blocking One Histo (NACALAI TESQUE; Kyoto, Japan) was dropped on the 5-μm thick sections that had been rinsed with PBS and were incubated for 5 min at room temperature. Next, they were rinsed with DW and left to react for 30 min with Normal Horse serum (2.5%, Vector Laboratories). After washing them with TBS, osteopontin (Anti-osteopontin Polyclonal Antibody, [bs-0026R] in TBS, 100-fold diluted, Bioss Inc. USA) was dropped on each section as the primary antibody and were left to react for 24 h at 4°C. After washing them with TBS, the secondary antibody (VectaFluor DyLight 488 Horse Anti-Rabbit IgG) was dropped on the sections and was left to react for 30 min at 37°C. After washing the specimens with TBS, they underwent nuclear staining for 1 min with DAPI and were then mounted with the designated mounting medium (VECTASHIELD Antifade Mounting Medium). Similar staining was also performed with osteocalcin (Anti-Osteocalcin Polyclonal Antibody [bs-4917R] in TBS, 100-fold diluted, Bioss Inc. USA) and Collagen I (Anti-Collagen I Polyclonal Antibody [bs-10423R] in TBS, 100-fold diluted, Bioss Inc. USA). The stained sections were observed with a fluorescence microscope (BX-53F, Olympus Co. Ltd., Japan) and the images were processed with a graphic software (Adobe Photoshop, Adobe Inc., USA)

***Elemental analysis***

For elemental analysis using electron probe micro-analyzer (EPMA, JXA-8900RL, JEOL Co. Ltd., Japan), 3-μm thick sections were used. The frozen sections were thawed and soaked in 100% ethanol 10 s later. Then, 60 s later, they were removed and dried. Next, the sections were fixed to an EPMA sample stage with a double-sided adhesive tape and coated with gold (Quick Auto Coater, Sanyu Denshi Co. Ltd., Japan). The elements in the section were analyzed using energy dispersive spectrometry (EDS) attached to the EPMA, and then calcium distribution images were collected using wavelength-dispersive X-ray spectroscopy (WDX).

***Cell count measurement***

We counted the number of newly formed cells in the blood clot that had formed at 3 days after the titanium foil implantation for three of the sections. DAPI-stained sections were used for cell count measurements. As shown in Fig. 3, we counted the number of cells in the blood clot surface layer (A1), central section (A2), and deep portion (A3: titanium

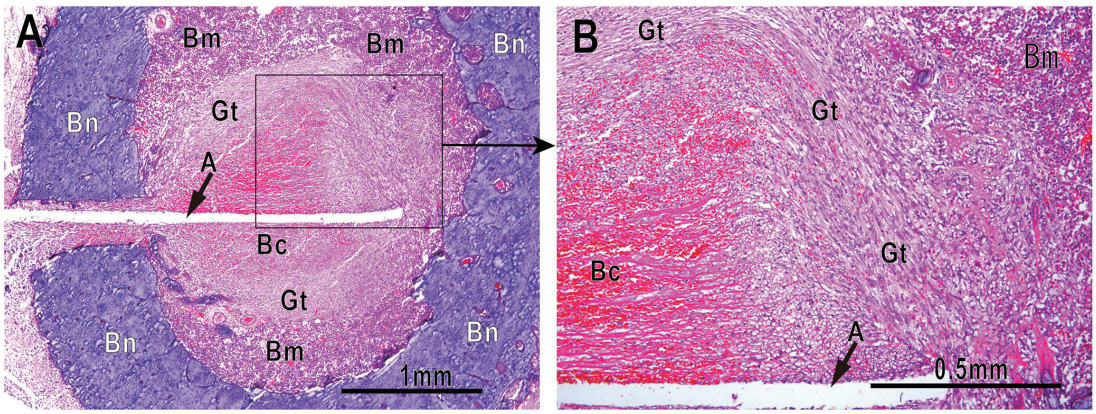


Figure 3. A: Frozen section from rat femur 5 days after the titanium foil implantation. The section thickness: 3 μm, H&E (Hematoxylin and eosin) staining, B: Enlarged view, Arrow A: Titanium foil implantation position, Bn: Bone, Bm: Marrow, Bc: Blood clot, Gt: Granulation tissue

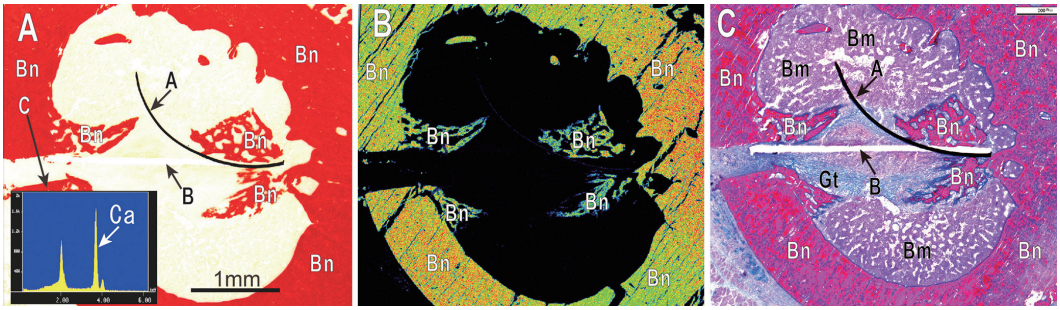


Figure 4. Calcium distribution in the frozen section of rat femur 7 days after the titanium foil implantation. The section thickness: 3 μm. A: Alizarin Red S staining (arrow C in the inserted figure shows the elemental analysis results), B: Ca distribution (EPMA), C: Masson trichrome staining (arrow A: titanium foil, arrow B: titanium foil implantation position), Bn: Bone, Bm: Bone marrow, Gt: Granulation tissue

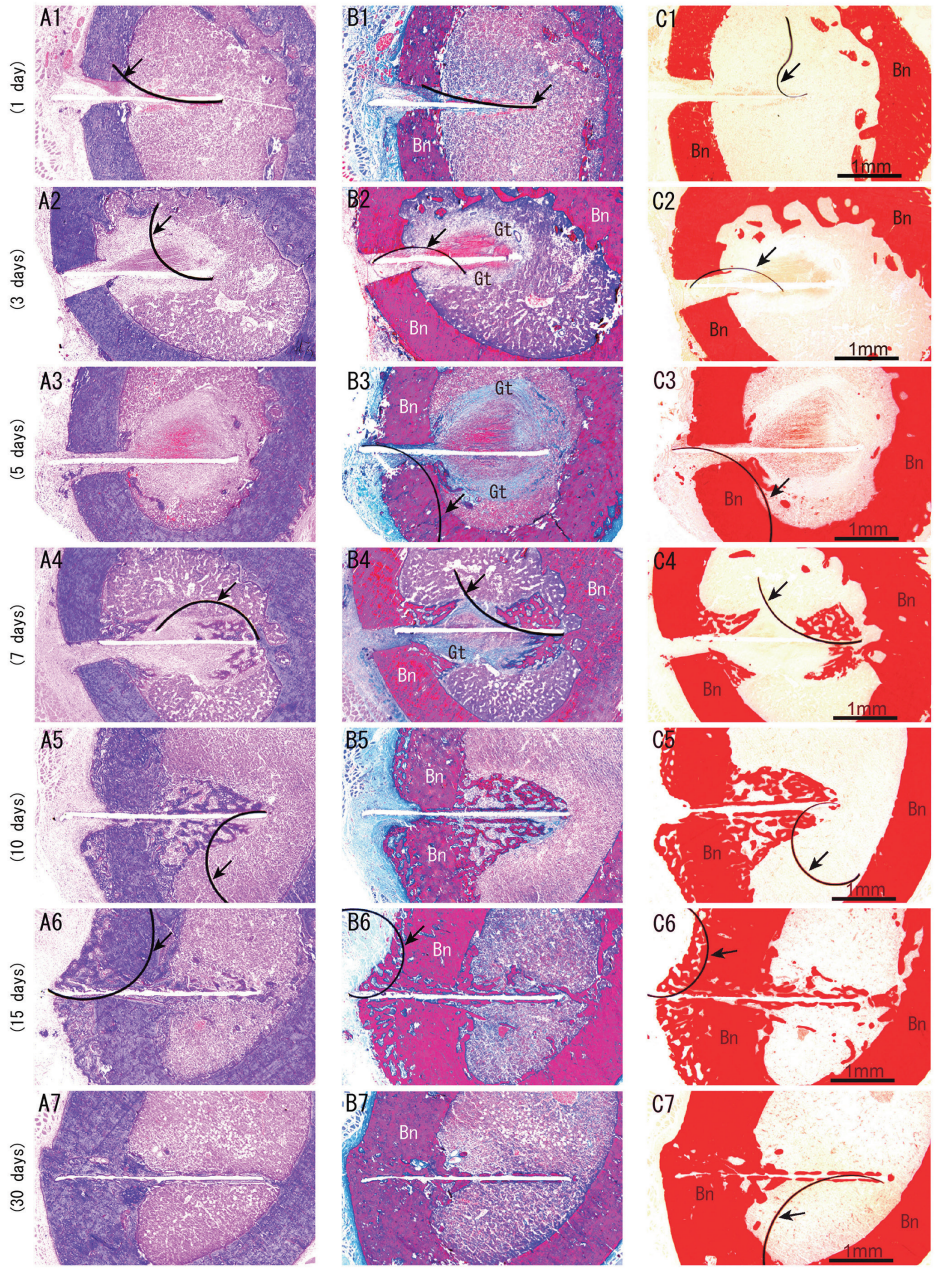


Figure 5. Histological changes in rat femurs implanted with titanium foil over time (1, 3, 5, 7, 10, 15, and 30 days after the titanium foil implantation). The section thickness: 3 μm, H&E staining (A1-7), Masson trichrome staining (B1-7), Alizarin Red S staining (C1-7), arrow: Titanium foil, Bn: Bone, Bm: Marrow, Bc: Blood clot, Gt: Granulation tissue

foil side). We calculated cell counts per unit area ($10^4$ μm$^2$) and the counting was performed with 3 sections.

## Results

### *Preparation of frozen sections*

We were able to prepare good frozen sections with a 3-μm thickness from non-decalcified frozen femur specimens into which the titanium foil had been implanted (Fig. 2). Although the titanium foil curled up while it was being cut and had moved from the implantation site, the histology of tissues around the titanium foil had almost perfectly preserved on the Cryofilm. Cells and bone were observe in the section clearly (Fig. 3).

### *Histological changes at the titanium foil implantation site over time*

Fig. 4 shows the results for Alizarin Red S staining, elemental analysis (EDS) with EPMA, calcium distribution images (WDS), and Masson trichrome staining of the serial undecalcified frozen sections at 7 days after the titanium implantation. EDS detected calcium in the areas that were stained red by Alizarin Red S staining (Fig. 4-A). The areas stained red by Alizarin Red S staining matched the areas in which WDS detected calcium distribution (Fig. 4-A, B). The areas stained in reddish purple by Masson trichrome staining was similar to the pattern of Alizarin Red S staining (Fig. 4-A, C).

Fig. 5 shows the histological changes in the tissue and the bone formed around the titanium over time after titanium foil implantation.

At 1 day after the titanium foil implantation, the area around the titanium foil was covered in blood from bleeding caused by the implantation procedure. Few cells and fibers stained with Masson trichrome were observed at the area (Fig. 5-A1, B1).

At 3 days after the implantation, the blood around the titanium foil had formed a clot (Fig. 5-A2, B2). Masson trichrome staining revealed fiber formation that stained blue in the superficial layer of the blood clot adjacent to the myeloid cells. Several cells were observed between the fibers and were found to be positive for ALPase. Alizarin Red S staining did not reveal any calcium precipitation in the granulation tissue (Fig. 5-C2).

At 5 days after the implantation, the superficial layer of the blood clot had formed granulation tissue (Fig. 5-A3, B3). The density of fiber bundles stained with Masson trichrome in the outer layer of the granulation tissue had increased, with some areas exhibiting bony tissue findings. While some fibers were also observed to be stained with trichrome in the blood clot near the titanium foil, the amount was lower than in the superficial layer.

At 7 days after the implantation, the blood clot had almost entirely been replaced by granulation tissue, and the range of fibers that were intensely stained with Masson trichrome had spread to cover the entire area of granulation tissue. The bony structure had expanded from the fibers in the outer circumference of the granulation tissue toward the titanium foil (Fig. 5-A4, B4, C4). The amount of fibers had also increased near the titanium foil (Fig. 5-C4).

At 10 days after the implantation, we observed bony tissue around the entire circumference of the granulation tissue. A cancellous bone-like structure had formed covering the titanium foil (Fig. 5-B5, C5 and Fig. 6-A1, B1). Bone formation around the titanium foil was completed by 10 days and osteoclasts were distributed on the surface of new formed bone almost equally. However, 10 days after the implantation, a lot of TRAPase-positive cells were distributed on the bone surface of the superficial layer near the bone marrow mainly (Fig. 6-A1, B1).

At 15 days after the implantation, the remarkable bone resorption was observed in the marrow side (Fig. 6-A2, B2). However, only a slight amount of bone resorption was observed near the titanium foil (Fig. 5-B6, C6 and Fig. 6-A2, B2).

At 30 days after the implantation, further resorption of the marrow side was observed, and the area had been replaced with myeloid cells excluding the bone tissue around the titanium foil and the bone only remained around the titanium foil (Fig. 5-A7, C7 and Fig. 6-A3, B3).

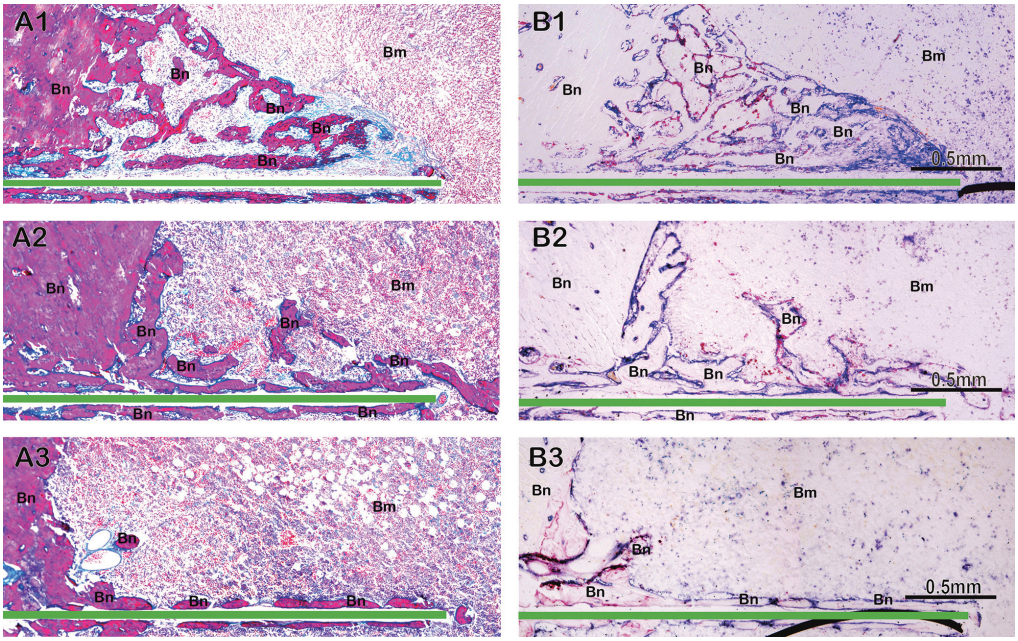


Figure 6. TRAPase activity on the new bone formed around the titanium foil. (A1, A2, A3: Masson trichrome staining, B1, B2, B3: ALPase [blue] and TRAPase staining [red]), A1, B1: At 10 days after the titanium implantation, A2, B2: At 15 days after the titanium implantation, A3, B3: At 30 days after the titanium implantation, the titanium foil implantation position is shown in green, Bn: Bone, Bm: Marrow

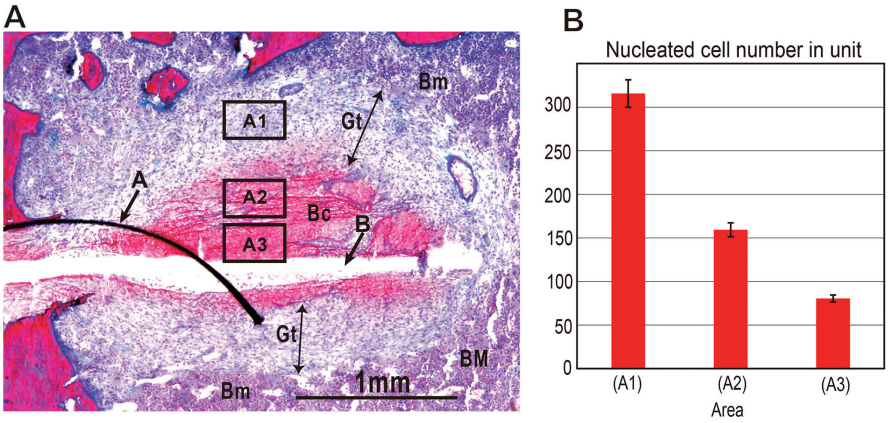


Figure 7. Proliferated cell numbers in granulation tissue of rat femur 3 days after titanium foil implantation. A1, A2 and A3 show the measured areas on the section (Masson trichrome staining). B: Measurement results, Arrow A: titanium foil, Arrow B: titanium foil implantation position, Bm: Bone marrow, Bc: Blood clot, Gt: Granulation tissue

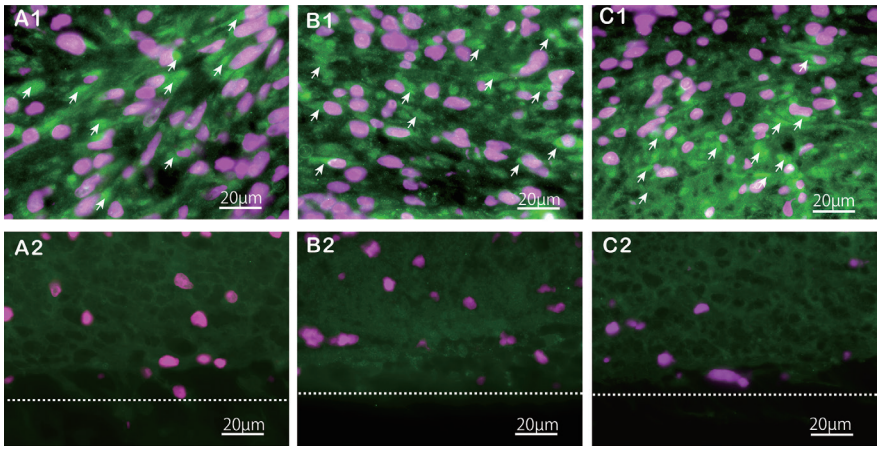


Figure 8. Immunohistochemical staining of rat femur frozen sections at 3 days after the titanium foil implantation. A1, A2: Osteopontin, B1, B2: Osteocalcin, C1, C2: Collagen type I (purple: nucleus, green: immune reaction). A1, B1, C1: bone marrow side of granulation tissue, A2, B2, C2: granulation tissue near the titanium, arrows show immune reaction. Dot line: the surface of implanted titanium foil.

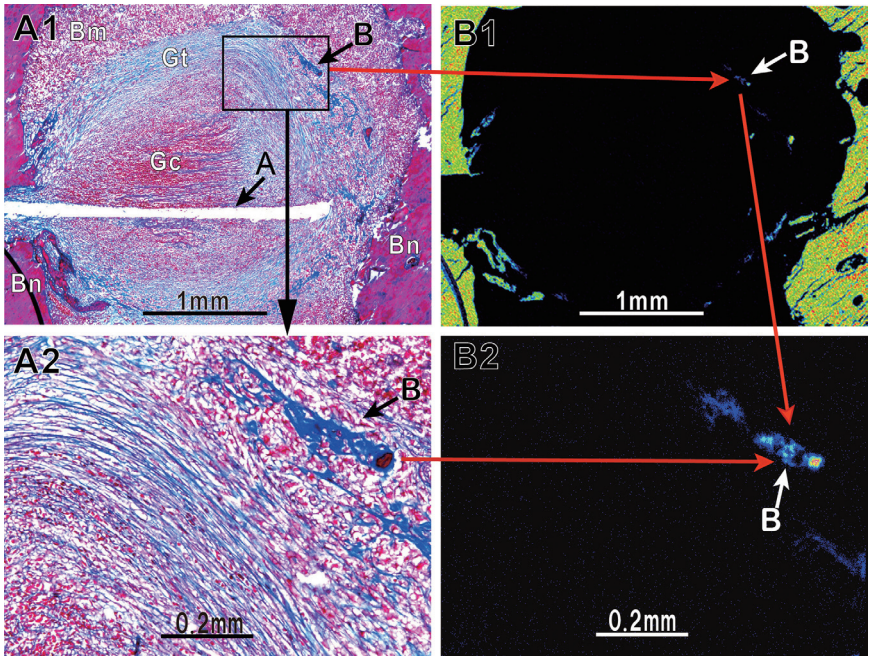


Figure 9. Masson trichrome staining (A1, A2) and calcium mapping image by EPMA (B1, B2). These results are prepared with serial 3μm thick sections. Arrow A: titanium foil implantation position, arrow B: initially calcified site. Bm: Bone marrow, Bc: Blood clot, Gt: Granulation tissue.

***Cell distribution***

The cell count in the blood clot 3 days after the titanium foil implantation was measured according to site using DAPI staining (Fig. 7). The highest cell count was noted in the superficial layer (marrow side) of the blood clot. However, there were few cells in the blood clot near the titanium foil, with a cell count of only one-quarter of that in the superficial layer of the blood clot.

***Immunohistochemistry***

The figure 8 shows immune-reaction of osteopontin, osteocalcin, and collagen type I on the specimen at 3 days after the titanium foil implantation. Clear positive reactions were observed in the marrow side cells for all the antibodies (Fig. 8-A1, B1, C1). However, a similar positive reaction was rarely observed for the cells in the granulation tissue that had formed around the titanium foil (Fig. 8-A2, B2, C2).

***Initially calcified site***

As shown in the figure 5-B2, the calcium precipitation was not detected on the fiber formed in the superficial layer of the blood clot at 3 days after titanium implantation. However, the calcium precipitation was clearly observed on the area at 5 days after the implantation. The figure 9 shows the site detected calcium precipitation and it shows clearly the calcium precipitation on the fibers stained with Masson trichrome staining (Fig. 9-A2, B2).

## Discussion

Titanium is the most widely used implant material. Its utility has been evaluated based on bone formation volume according to X-ray and micro-CT findings. In terms of its biocompatibility, studies have investigated the adhesion of cells to titanium and close adhesion to bony tissue[36-38]. However, the histological changes around titanium directly after implantation, which are the most important factors for determining the process of bone formation around the titanium, have yet to be elucidated due to technical issues. It is best to use frozen sections to enable histochemical and immunohistochemical investigations as well as genetic analysis to clarify the histological changes that occur immediately after titanium implantation. The first aim of this study is to prepare the undecalcified frozen sections from titanium implantation tissues and to demonstrate that the sections are usable for histological, histochemical and immune-histochemical studies.

It is known that it is impossible to make frozen sections from tissues including bulk titanium used for implantation. However, extensive useful information related to implantation will be obtained if the preparation of frozen sections becomes possible. We introduced a titanium foil in this study to achieve this purpose. This present study clearly showed that it was relatively simple to implant titanium foil of 30-μm thickness into rat femurs, and serial frozen sections of 3-μm thickness could be prepared from the undecalcified femurs containing titanium foil (Fig. 2). Although we faced the challenge of the titanium foil becoming wrinkled while it was cut and coming off from the Cryofilm, the tissue around the titanium foil had almost completely remained in place on the Cryofilm, and the soft and calcified tissue morphology was accurately maintained.

Histological images, including osteoblasts, osteoclasts and bone, could be observed clearly in the sections by tissue staining, such as H-E staining, Alizarin Red S staining, and Masson trichrome S staining (Fig. 5). In addition, ALPase staining and TRAPase staining showed changes clearly (Fig. 6). Furthermore, these specimens showed good stability against immunostaining with osteopontin, osteocalcin, and collagen type I (Fig. 8), and the distribution of calcium and similar structures could be evaluated using elemental analysis with EPMA (Figs. 4 and 9).

These findings demonstrate that the present method allows to study the titanium implant tissue using histological, histochemical, enzyme histochemical and immune-histochemical studies, and elemental analysis. Furthermore, the present sections are applicable for gene analysis by LMD technique and for studying the distribution of small molecules with mass spectrometry imaging. All the application is achieved on the serial sections made with same sample by this method although it is impossible to do it with conventional techniques. It means that the present method is useful for studying implant tissue greatly.

The second aim of this study is to define the bone formation process around the implanted titanium.

The induction potency of osteoprogenitor cells is known to be higher in the metaphysis region, including the long bone trabeculae, than in the diaphysis region[39]. To prevent this from affecting the results, titanium foil was implanted in the diaphysis region with no trabeculae. As previous reports have shown that bone tissue around the titanium forms within 30 days, we set the experiment period to 1–30 days after the titanium implantation to clarify bone tissue formation around the titanium[10].

The healing mechanism observed after titanium implantation into the bone marrow is described as follows. First, at 1 day after implantation, the area around the titanium foil was filled with blood from bleeding during implantation. At 3 days after the implantation, the blood around the titanium became a clot, and fibers were formed in the superficial layer adjacent to the bone marrow of the blood clot. The fibers were stained blue with Masson trichrome and found to be positive for collagen type I, indicating that they were collagen fibers. As the cell count was high for the bone marrow and low for the blood clot, it appeared that the cells were moving into the blood clot from the bone marrow side. Immunostaining for osteopontin, osteocalcin, and collagen type I revealed expression of all genes at 3 days after the implantation. Several osteopontin, osteocalcin, and collagen type I positive cells were found on the bone marrow side of the blood clot, and there were few cells around the titanium foil. Therefore, it is conceivable that cells form bone while moving toward the periphery of titanium while being differentiated and proliferated. At 5 days after the implantation, the blood clot turned into granulation tissue, and calcium precipitation appears on the fibers stained with Masson trichrome in the granulation tissue area of the marrow side. At 7 days after the implantation, fibrosis had progressed, and bone formation started in the superficial layer of the granulation tissue. At 10 days after the implantation, the calcified area had expanded close to the titanium and calcified tissue was observed throughout the granulation tissue. Then, a large number of osteoclasts appeared on the bone surface of the marrow side of the calcified tissue, and bone resorption was observed. At 15 days after the implantation, heavy bone resorption was observed on the bone of marrow side though the resorption was little on the bone near the titanium. At 30 days after the implantation, bone resorption on the marrow side had progressed further. Ultimately the bone was left only in the area around the titanium foil.

These results clearly show that bone formation around the titanium occurs in the following process. The blood from bleeding caused by titanium implantation forms a blood clot. 3 days after implantation, osteoblasts and fibroblasts, proliferate in it, synthesize and secrete bone matrix proteins, such as collagen fibers, while also promoting blood clot resorption. 5 days after implantation, calcium precipitates on the collagen fibers formed in this granulation tissue, starting the calcification process. Calcification spreads throughout the entire area of the granulation tissue and new bone forms. Next, new bone resorption starts from

the marrow side. The new bone is resorbed except for the bone tissue around the titanium and, finally, the titanium becomes more stabilized by the bone tissue remaining around it.

**Conflict of Interest**

There is no conflict of interest.

**References**


1. Yoshioka N and Tominaga S. Titanium mesh implant exposure due to pressure gradient fluctuation. World Neurosurg 119: e734-e739, 2018
2. Sultan A, Bhat MR, Khursheed O, Wani MM, Kawoosa AA, Kotwal HA and Manzoor QW. Evaluation of complications from stainless-steel flexible intramedullary nailing in children's femoral shaft fractures and recommendations for continued use. Ortop Traumatol Rehabil 19(3): 263-271, 2017
3. Sabah Y, Clément JL, Solla F, Rosello O and Rampal V. Cobalt-chrome and titanium alloy rods provide similar coronal and sagittal correction in adolescent idiopathic scoliosis. Orthop Traumatol Surg Res 104(7): 1073-1077, 2018
4. McGlumphy E, Brantley W and Johnston WM. *In vitro* fit of CAD-CAM complete arch screw-retained titanium and zirconia implant prostheses fabricated on 4 implants. J Prosthet Dent 119(3): 409-416, 2018
5. Steiger-Ronay V, Krcmaric Z, Schmidlin PR, Sahrmann P, Widedemeier DB and Benic G. Assessment of peri-implant defects at titanium and zirconium dioxide implants by means of periapical radiographs and cone beam computed tomography: An *in-vitro* examination. Clin Oral Implants Res 29(12): 1195-1201, 2018
6. Menini M, Pesce P, Pera F, Barberis F, Lagazzo A, Bertoa L and Pera P. Biological and mechanical characterization of carbon fiber frameworks for dental implant applications. Mater Sci Eng C Mater Biol 70: 646-655, 2017
7. Vallittu PK, Närhi TO and Hupa L. Fiber glass-bioactive glass composite for bone replacing and bone anchoring implants. Dent Mater 31(4), 371-381, 2015
8. Hayakawa T, Takahashi K, Okada H, Yoshinari M, Hara H, Mochizuki C, Yamamoto H and Sato M. Effect of thin carbonate-containing apatite (CA) coating of titanium fiber mesh on trabecular bone response. J Mater Sci Mater Med 19(5): 2087-2096, 2008
9. Alkharrat AR, Schmitter M, Rues S and Rammelsberg P. Fracture behavior of all-ceramic, implant-supported, and tooth-implant-supported fixed dental prostheses. Clin Oral Investig 22(4): 1663-1673, 2018
10. Suzuki T, Hayakawa T, Kawamoto T and Gomi K. Bone response of TGF-b2 immobilized titanium in a rat model. Dent Mater J 33: 233-241, 2014
11. Yan J, Chang B, Hu X, Cao C, Zhao L and Zhang Y. Titanium implant functionalized with antimiR-138 delivered cell sheet for enhanced peri-implant bone formation and vascularization. Mater Sci Eng C Mater Biol Appl 89, 52-64, 2018
12. Dayan A, Lamed R, Benayahu D and Fleminger G. RGD-modified dihydrolipoamide dehydrogenase as a molecular bridge for enhancing the adhesion of bone forming cells to titanium dioxide implant surfaces. J Biomed Mater Res A 107(3): 545-551. 2019
13. Iaculli F, Di Filippo ES, Piattelli A, Mancinelli R and Fulle S. Dental pulp stem cells grown on dental implant titanium surfaces: An *in vitro* evaluation of differentiation and microRNAs expression. J Biomed Mater Res B Appl Biomater 105(5): 953-965, 2017
14. Piattelli A, Corigliano M, Scarano A, Costigliola G and Paolantonio M. Immediate loading of titanium plasma-sprayed implants: a histologic analysis in monkeys. J Periodontol 69(3): 321-327, 1998
15. Scarano A, Lorusso F, Orsini T, Morra M, Iviglia G and Valbonetti L. Biomimetic surfaces coated with covalently immobilized collagen type I: An x-ray photoelectron spectroscopy, atomic force microscopy, micro-ct and histomorphometrical study in rabbits. Int J Mol Sci 20(3): 724, 2019
16. Van Dijk IA, Beker AF, Jellema W, Nazmi K, Wu G, Wismeijer D, Krawczyk PM, Bolscher JGM, Veerman EC and Step J. Histatin 1 enhances cell adhesion to titanium in an implant integration model. J Dent Res 96(4): 430-436, 2017
17. Li X, Xue W, Cao Y, Long Y and Xie M. Effect of lycopene on titanium implant osseointegration in ovariectomized rats. J Orthop Surg Res 13(1), 237, 2018
18. Liu D, He C, Liu Z and Xu W. Gentamicin coating of nanotubular anodized titanium implant reduces implant-related osteomyelitis and enhances bone biocompatibility in rabbits. Int J Nanomedicine 12: 5461-5471, 2017
19. Korn P, Schulz MC, Hintze V, Range U, Mai R, Eckeit U, Schnabelrauch M, Möller S, Becher J, Scharnweber D and Stadlinger B. Chondroitin sulfate and sulfated hyaluronan-containing collagen coatings of titanium implants influence peri-implant bone formation in a minipig model. J Biomed Mater Res A 102(7): 2334-2344, 2014
20. Stokholm R, Isidor F and Nyengaard JR. Histologic and histomorphometric evaluation of peri-implant bone of immediate or delayed occlusal-loaded non-splinted implants in the posterior mandible-an experimental study in monkeys. Clin Oral Implants Res 25(11): 1311-1318, 2014
21. Wang S, Ogawa T, Zheng S, Miyashita M, Tenkumo T, Gu Z, Lian W and Sasaki K. The effect of low-magnitude high-frequency loading on peri-implant bone healing and implant osseointegration in Beagle dogs. J Prosthodont Res 62(4): 497-502, 2018
22. Sennerby L, Thomsen P and Ericson LE. A morphometric and biomechanic comparison of titanium implants inserted m rabbit cortical and cancellous bone. Int J Oral Maxillofac Implants 7(1): 62-71, 1992
23. Evans GH, Mendez AJ and Caudill RF. Loaded and nonloaded titanium versus hydroxyapatite-coated threaded implants in the canine mandible. Int J Oral Max1llofac Implants 11(3): 360-371, 1996
24. Yu YJ, Zhu WQ, Xu LN, Ming PP, Shao SY and Qiu J. Osseointegration of titanium dental implant under fluoride exposure in rabbits: Micro-CT and histomorphometry study. Clin Oral Implants Res 30(10): 1038-1048, 2019
25. Scarano A, Iezzi G, Petrone G, Marinho VC, Corigliano M and Piattelli A. Immediate postextraction implants: a histologic and histometric analysis in monkeys. J Oral Implantol 26(3): 163-169, 2000
26. Rousselle SD, Wicks JR, Tabb BC, Tellez A and O'Brien M. Histology strategies for medical implants and interventional device studies. Toxicol Pathol 47(3): 235-249, 2019
27. Kawamoto T. Use of a new adhesive film for the preparation of multi-purpose fresh-frozen sections from hard tissues, whole-animals, insects and plants. Arch Histol Cytol 66(2): 123-143, 2003
28. Kawamoto T and Kawamoto K. Preparation of thin frozen sections from nonfixed and undecalcified hard tissues using Kawamot's film method (2012). Methods Mol Biol 1130: 149-164, 2014
29. Morodomi Y, Kanaji S, Won E, Kawamoto T and Kanaji T. Modified application of Kawamoto's film method for super-resolution

imaging of megakaryocytes in undecalcified bone marrow. Res Pract Thromb Haemost 4(1): 86-91, 2020
30. Saigusa D, Saito R, Kawamoto K, Uruno A, Kano K, Aoki J. Yamamoto M and Kawamoto T. Conductive adhesive film expands the utility of matrix-assisted laser desorption/ionization mass spectrometry imaging. Anal Chem 91(14): 8979-8986, 2019
31. Takimoto A, Kawatsu M, Yoshimoto Y, Kawamoto T, Seiryu M, Yamamoto TT, Hiraki Y and Shukunami C. Scleraxis and osterix antagonistically regulate tensile force-responsive remodeling of the periodontal ligament and alveolar bone. Development 142(4): 787-796, 2015
32. Arima Y, Harada M, Kamimura D, Park JH, Kawano F, Yull FE, Kawamoto T, Iwakura Y, Betz UAK, Marquez G, Blackwell TS, Ohira Y, Hirano T and Murakami M. Regional neural activation defines a gateway for autoreactive T cells to cross the blood-brain barrier. Cell 148(3): 447-457, 2012
33. Masson P. Some histological methods: Trichrome staining and their preliminary technique. J Tech Methods 12: 75, 1929
34. Martinello T, Pascoli F, Caporale G, Perazzi A, Iacopetti I and Patruno M. Might the Masson trichrome stain be considered a useful method for categorizing experimental tendon lesions? Histol Histopathol 30(8): 963-969, 2015
35. Burstone MS. The relationship between fixation and techniques for the histochemical localization of hydrolytic enzymes. J Histochem Cytochem 6(5): 322-339, 1958
36. Souza AB, Alshihri A, Kämmerer PW, Araujo MG and Gallucci GO. Histological and micro-CT analysis of peri-implant soft and hard tissue healing on implants with different healing abutments configurations. Clin Oral Implants Res 29(10): 1007-1015, 2018
37. Bissinger O, Probst FA, Wolff KD, Jeschke A, Weitz J, Deppe H and Kolk A. Comparative 3D micro-CT and 2D histomorphometry analysis of dental implant osseointegration in the maxilla of minipigs. J Clin Periodontol 44(4): 418-427, 2017
38. Yu YJ, Zhu WQ, Xu LN, Ming PP, Shao SY and Qiu J. Osseointegration of titanium dental implant under fluoride exposure in rabbits: Micro-CT and histomorphometry study. Clin Oral Implants Res 30(10): 1038-1048, 2019
39. Davies JE. Understanding peri-implant endosseous healing. J Dent. Educ 67(8): 932-949, 2003